Thermomechanical Behavior and Local Dynamics of Dendronized Block Copolymers and Constituent Homopolymers

ARTICLE *in* MACROMOLECULES · JUNE 2015

Impact Factor: 5.8 · DOI: 10.1021/acs.macromol.5b00779

Macromolecules

Article

pubs.acs.org/Macromolecules

Thermomechanical Behavior and Local Dynamics of Dendronized Block Copolymers and Constituent Homopolymers

A. Aluculesei,[†] A. Pipertzis,[‡] V. A. Piunova,[§] G. M. Miyake,[§] G. Floudas,[‡] G. Fytas,*[,†,∥] and R. H. Grubbs[§]

[†]Department of Materials Science, FORTH-IESL, P.O. Box 1527, 71110 Heraklion, Greece

[‡]Department of Physics, University of Ioannina, 45110 Ioannina, Greece

[§]Arnold and Mabel Beckmam Laboratories for Chemical Synthesis, Division of Chemistry and Chemical Engineering, California Institute of Technology, Pasadena, California 91125, United States

[∥]Max Planck Institute for Polymer Research, D-55128 Mainz, Germany

Supporting Information

ABSTRACT: We employ Brillouin light scattering (BLS) and dielectic spectroscopy (DS) to study the phononic behavior, thermomechanical properties, and segmental dynamics of symmetric block copolymers (BCP) constructed from discrete wedge-type repeat units and the corresponding dendronized constituent homopolymers over a broad temperature range. In spite of the sufficiently large elastic contrast between the bulk homopolymers, for the BCPs an absence of a bandgap in the phonon dispersion relation along the periodicity direction implies different modified sound velocities in the photonic BCP lamellar films. The anticipated rich segmental dynamics reveal interfacial mixing as well as confinement effects of the two blocks. This class of amorphous dendronized homopolymers and BCPs reveal strong effects of the wedge-like side groups manifested in the vastly different glass transition temperatures (T_g), free-volume domination of the temperature dependence of the elastic modulus, and heterogeneous segmental dynamics represented by four relaxation processes.

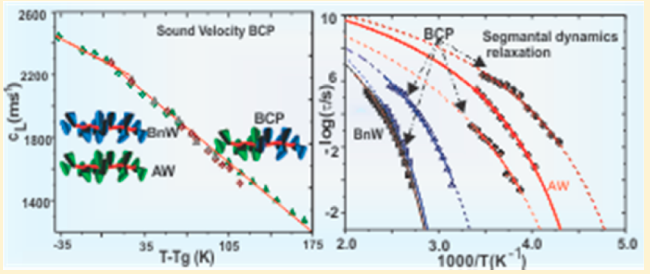

I. INTRODUCTION

The self-assembly of block copolymers (BCPs) can render highly ordered nanostructured materials with periodicity typically on the order of tens of nanometers.[1,2] If the optical periodicity of the material can match the path length of a photon, a photonic band gap can be formed that inhibits the propagation of certain wavelengths of light through the bulk.[3] Photonic crystals can be prepared through the self-assembly of BCPs; however, the complicated self-assembly of BCPs often presents an energy barrier to reorganization that greatly impedes assembly and restricts domain size.[4,5] Although domain size swelling can increase the wavelength of reflection,[6] we sought to design BCP architectures that could assemble to long wavelength reflectors without the need for additives. Through minimizing the BCP's ability to engage in chain entanglement, the reorganization to large domain sized nanostructured materials is facilitated.[7]

Specifically, we have been focusing on molecular brush and dendronized BCPs as a route to access one-dimensional photonic crystals through the self-assembly of BCPs. These copolymers consist of a polymeric main chain that unifies a densely packed array of bulky repeat units.[8] Congestion imparted by the repeat units enforces the polymer main-chain elongation with a low potential for chain entanglement.[9] Molecular brush copolymers can be synthesized by grafting-from, grafting-to, and grafting-through strategies.[10] Using ruthenium mediated ring-opening metathesis polymerization (ROMP), we have been interested in the grafting-through approach, directly polymerizing norbornene-functionalized macromonomers, ensuring that every repeat unit consists of a polymeric repeat unit, to well-defined brush BCPs.[11,12] These BCPs rapidly assembled to photonic crystals that reflected light from the UV, through the visible, and into the near-IR.[6,13] The peak wavelength of reflection (λ_{max}), and thus the periodicity of the nanostructured assembly, could be predictably controlled through synthetic tuning of the polymer molecular weight (MW). Despite the control over λ_{max}, the bandgaps of the photonic crystals were somewhat large, and increased with λ_{max}.

We partially attributed the large bandgaps to dispersity in the periodicity of the nanostructures. The molecular brush BCP architecture inherently incorporates three nonuniform components: the polymeric main chain and the two polymeric repeat units from each block. Although the dispersity in the polymer main chain cannot be eliminated, we hypothesized that if a BCP with low chain entanglement could be synthesized from discrete molecular building blocks, then it could assemble to a photonic crystal with a narrow bandgap. Dendronized polymers are a class of polymers that are constructed from

Received: April 15, 2015
Revised: May 19, 2015

DOI: 10.1021/acs.macromol.5b00779
Macromolecules XXXX, XXX, XXX−XXX

Scheme 1. Structures for the Alkyl (AW, Blue) and Benzyl (BnW, Green) Wedge Monomers and Diblock Copolymer

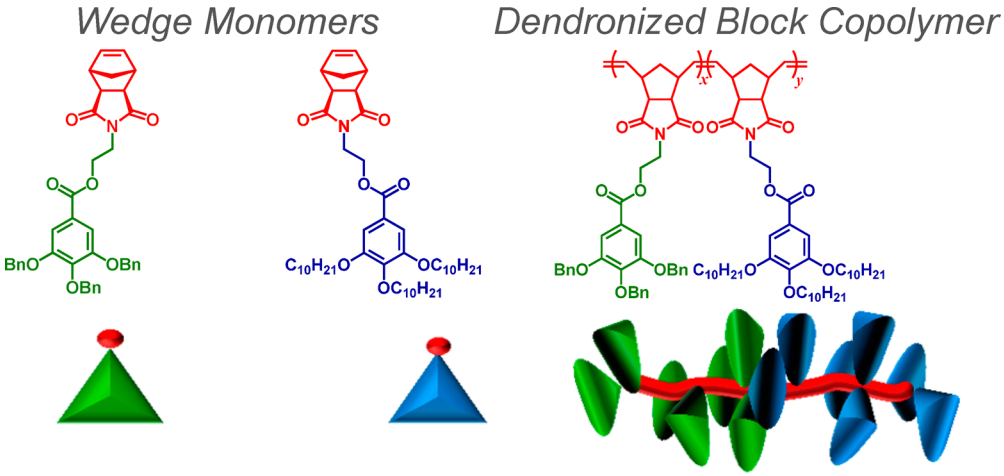

discrete wedge-type repeat units and exhibit reduced chain entanglement.[14,15] Using ruthenium-mediated ROMP, we sequentially polymerized wedge-type monomers to synthesize well-defined dendronized BCPs.[6] The dendronized BCPs assembled to 1D photonic crystals that reflected light across the visible spectrum and demonstrated narrowed bandgaps in comparison to their molecular brush BCP analogues.

The motivation for the present study was twofold: examine whether the dendronized BCPs also exhibit phononic band gap which should fall in the hypersonic (GHz) frequency range[16] and investigate the local structure and dynamics of this new class of polymers with unexplored physical properties. The anticipated bulky "wedge"-like side groups (Scheme 1) and the type of substituents (alkyl wedge [AW] and benzyl wedge [BnW]) should significantly affect the packing in the solid rubbery and glassy states of the dendronized homopolymers and BCPs that can impact the local dynamics and thermomechanical properties as compared to conventional amorphous polymers.[17,18] We have therefore performed Brillouin light scattering (BLS) to record the phononic dispersion relation and the temperature dependence of the longitudinal elastic modulus below and above the softening transition. The scattering wave vector can be directed along and normal to the periodicity direction, and the phonon wavelength can provide space resolution in the submicrometer range that is necessary to match the structure periodicity and also measure the effective medium elastic properties of the BCP stack. Furthermore, owing to the finite dipole moment of the monomer units, dielectric spectroscopy (DS) reports on the local dynamics below and above the two glassy states of BCPs in comparison to the constituent homopolymers.

All BCPs examined are in the microphase-separated regime up to the highest examined temperature (~410 K) exhibiting two very different T_gs (233 K for the AW block and 360 K for the BnW block, with the former being very broad) associated with the constituent homopolymers. In spite of sufficiently large elastic mechanical contrast due to the T_g disparity, the photonic BCPs are unexpectedly not unidirectional hypersonic band gap materials. The elastic longitudinal modulus is dictated by an effective T_g intermediate of the two constituent homopolymers. Segmental dynamics of the microphase separated BCPs associated with the two T_{gs} reveal different dynamic processes associated with confinement effects as well as interfacial mixing. The paper proceeds with the experimental techniques in section II, the sound propagation along and normal to the periodicity direction of BCPs in subsection IIIA, and the temperature dependence of the sound velocity in subsection IIIB. The segmental dynamics of the BCP's block components are presented in subsection IIIC, and the paper concludes with section IV.

II. EXPERIMENTAL SECTION

Samples. The synthesis of the homopolymers and BCPs used in the present study is described elsewhere.[7] The molecular weight, the polydispersity, and the lamellar spacing are listed in Table 1. The

Table 1. Molecular Weight Properties of the Polymers Investigated in This Study and the Domain Sizes of the Assembled Block Copolymers

sample	M_w[a] (kDa)	PDI[a] (M_w/M_n)	thickness[b] BnW/AW (nm)
BCP	480[c]	1.05	40/50
	570	1.05	90/72
	1250	1.10	154/124
	1390	1.24	340/274
	3123	1.58	not measured
BnW	544	1.15	
	789	1.03	
AW	445	1.03	

[a]Measured by light scattering. [b]Measured by scanning electron microscopy. Samples 1−3 were prepared by controlled evaporation from dichloromethane. [c]The sample was thermally annealed for 24 h at 100 °C.

polymer films were deposited on glass slides, previously washed with methanol and hexanes, through controlled evaporation from dichloromethane (2 g/L). The dry coatings were thermally annealed in a vacuum oven at 100 °C for 24 h.

Brillouin Light Scattering (BLS). The phonon dispersion frequency (ω) vs wave vector (q) was obtained from the BLS spectrum, $I(q,\omega)$, recorded by a high-resolution six-path tandem Fabry−Perot interferometer.[1] Two phonon propagations parallel and normal to the film plane (left panel of Figure 1) were selected utilizing the scattering geometries shown in Figure 1. In the transmission geometry (middle panel) and for an incidence angle $\alpha = \theta/2$, the amplitude $q_{\parallel} = (4\pi/\lambda)\sin(\theta/2)$ is independent of the refractive index (n) of the film; λ is the wavelength of the laser light, and θ is the scattering angle between the wave vectors k_i and k_s of the incident laser beam and the scattered by the phonon light, respectively; hence, the phonon wavelength is $q = k_s - k_i$ In the reflection geometry (right

DOI: 10.1021/acs.macromol.5b00779
Macromolecules XXXX, XXX, XXX−XXX

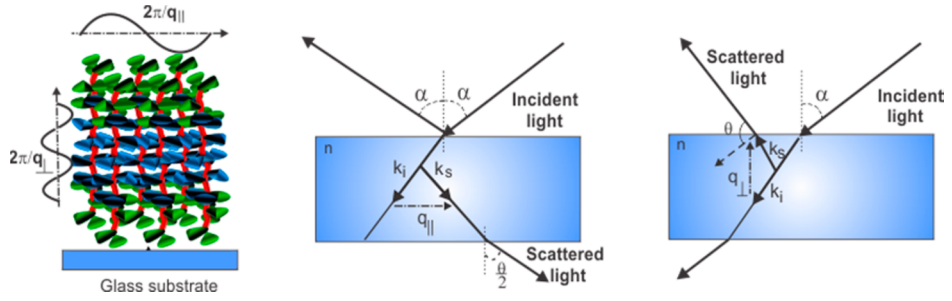

Figure 1. Illustration of one-dimensional bilayer structure of a supported symmetric dendronized diblock copolymer. Phonon propagation normal to ($q_\perp$) and parallel ($q_\parallel$) to the substrate is probed using the two light scattering geometries of the middle and right panel. The direction of $q_\perp$ and $q_\parallel$ are along and normal to the periodicity direction, respectively. Along the periodicity, phonon wavelength and spacing are comparable, whereas parallel to the lamellae the phonon propagation is probed at a longer wavelength.

panel of Figure 1), the amplitude $q_\perp$ depends on n. Along this (periodicty) direction, the phonon wavelength matches the spacing in the BCP-480. For the temperature-dependent study BLS spectra were recorded at a single scattering angle $\theta = 90°$, at which the phonon wavelength $2\pi/q_\parallel$ is larger than the spacing. In this case, the phonon propagation in the effective medium is probed.

Differential Scanning Calorimetry (DSC). A Q2000 (TA Instruments) was used for thermal analysis with a cooling/heating rate of 10 K/min at a temperature range from 153 to 413 K. The instrument was calibrated for best performance on the specific temperature range and heating/cooling rate. The calibration sequence included a baseline calibration for the determination of the time constants and capacitances of the sample and reference sensor using a sapphire standard, an enthalpy and temperature calibration for the correction of thermal resistance using indium as standard (ΔH = 28.71 J/g, T_m = 428.8 K), and a heat capacity calibration with sapphire standard. The DSC traces from the second heating run shown in Figure 2 depict two T_gs in the copolymers that nicely correspond to

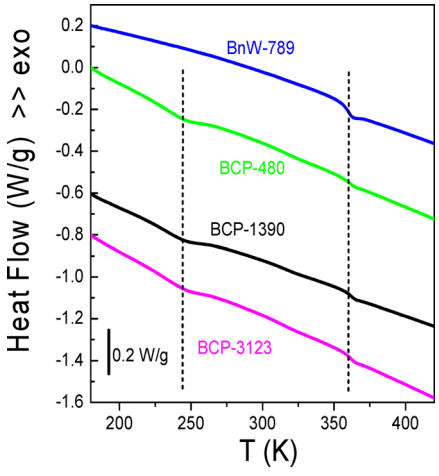

Figure 2. DSC traces of the BnW homopolymer and four block copolymers as indicated. Traces refer to the second heating run with a rate of 10 K/min.

the respective homopolymers suggesting microphase separation. The glass temperatures and change in specific heat at the respective T_g are shown in Table 2.

Dielectric Spectroscopy (DS). The sample cell consisted of two electrodes, 20 mm in diameter and a thickness of 50 μm. Dielectric measurements were made at different temperatures in the range 253.15 to 423.15 K, at atmospheric pressure, and for frequencies in the range from 1×10^{-2} to 1×10^{6} Hz using a Novocontrol Alpha frequency analyzer with an active sample head. The complex dielectric permittivity $\varepsilon^* = \varepsilon' - i\varepsilon''$, where ε' is the real and ε'' is the imaginary part, is a function of frequency ω, temperature T, and in general

Table 2. Glass Temperatures (T_g) and Specific Heat Change (Δc_p) at the Respective Transition Measured with a Rate of 10 K/min

compound	$T_{g,1}$ (K)	$\Delta c_{p,1}$ (J/K)	$T_{g,2}$ (K)	$\Delta c_{p,2}$ (J/K)
BnW-789	360 ± 2	0.43		
BCP-480	360 ± 2	0.26	233 ± 8	0.14
BCP-1390	361 ± 2	0.21	234 ± 8	0.32
BCP-3123	361 ± 2	0.26	233 ± 8	0.33

pressure P, $\varepsilon^* = \varepsilon^*(\omega,T,P)$.[19,20] In the analysis of the DS spectra we have used the empirical equation of Havriliak and Negami (HN)[21]

$$\varepsilon^*_{HN}(\omega, T) = \varepsilon_\infty(T) + \frac{\Delta\varepsilon(T)}{[1 + (i\omega\tau_{HN}(T))^m]^n} + \frac{\sigma_0(T)}{i\varepsilon_f\omega} \quad (1)$$

where $\tau_{HN}(T,P)$ is the characteristic relaxation time, $\Delta\varepsilon(T,P) = \varepsilon_0(T,P) - \varepsilon_\infty(T,P)$ is the relaxation strength of the process under investigation, m and n (with limits $0 < m$, $mn \leq 1$) describe respectively the symmetrical and unsymmetrical broadening of the distribution of relaxation times, σ_0 is the dc conductivity, and ε_f is the permittivity of the free space. In the fitting procedure, we have used the ε'' values at every temperature, and in some cases the ε' data were also used as a consistency check. From, τ_{HN} the relaxation time at maximum loss, τ_{max}, is obtained analytically following

$$\tau_{max} = \tau_{HN} \sin^{-1/m}\left(\frac{\pi m}{2(1+n)}\right) \sin^{1/m}\left(\frac{\pi mn}{2(1+n)}\right) \quad (2)$$

In the temperature range where two relaxation processes contribute to ε^* there are two ways of representing the data. The first one, followed here, is based in a summation of two HN functions and assumes statistical independence in the frequency domain.

Optical Transmittance. A UV-241PC spectrometer operating in the range 200−800 nm was used to record the transmission spectrum of the film BCP-480 after the completion of the BLS experiment. The normal incidence UV−vis transmission spectrum has been acquired by illuminating a specific area of the surface of the thin film and collecting the transmission light within a small (∼1°−5°) solid angle.

III. RESULTS AND DISCUSSION

A. Phonon Propagation Normal and Parallel to the Periodicity Direction. Figure 3a displays the experimental BLS of the two homopolymers (BnW and AW) for propagation parallel to the substrate at $q_\parallel$ = 0.0167 nm^{-1}. The experimental spectra are well represented by a single Lorentzian shape (Figure 3, red line of the anti-Stokes side), and the phonon frequency, $\omega = 2\pi f$, at the peak maximum exhibts a linear acoustic, $\omega = cq_\parallel$, dependence (see Figure 4). The two homopolymers display significantly (∼25%) different frequencies (vertical dashed lines) with the glassy (at ambient

DOI: 10.1021/acs.macromol.5b00779
Macromolecules XXXX, XXX, XXX−XXX

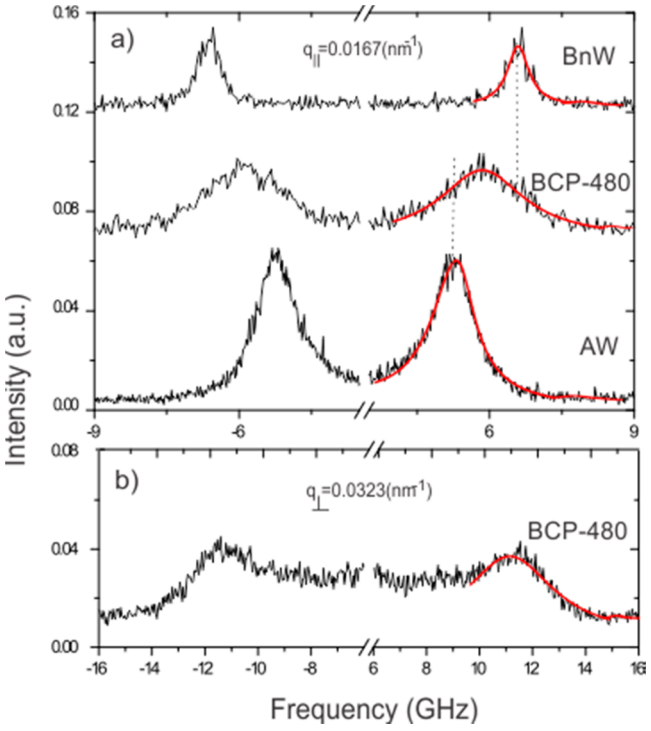

Figure 3. (a) Brillouin light scattering (BLS) spectra of the two dendronized homopolymers and BCP-480 at $q_{||}$ = 0.0167 nm^{-1} films and 20 °C. The two vertical dashed lines indicate the frequencies at the peak of the BLS spectra of the two homopolymers recorded at the same $q_{||}$. (b) BLS spectrum of BCP-480 recorded with $q_{\perp}$ along the periodicity direction. Solid lines on the anti-Stokes side denote the representation of the BLS spectrum by a single Lorentzian line shape.

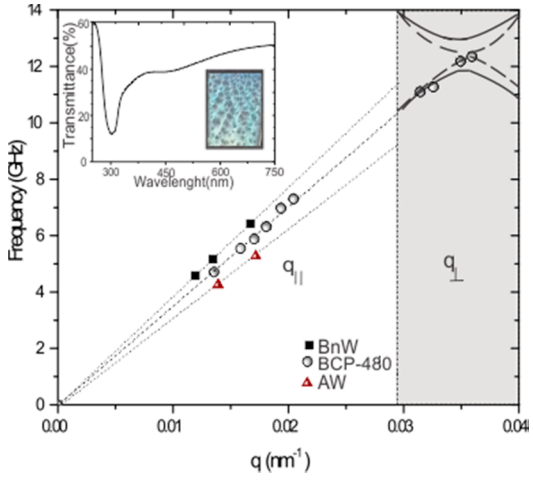

Figure 4. Dispersion relation for phonon propagation normal ($q_{||}$, open circles) and along ($q_{\perp}$, solid circles in the shaded region) to the periodicity direction for the BCP-480 supported film with lattice constant, d = 90 nm. The purely acoustic behavior of the two constituent homopolymers with c_1 = 1985 m/s (AW-445) and c_2 = 2485 m/s (BnW-544) is also shown. The theoretical band diagram along the periodicity of the film is computed with either c_1 = 1985 m/s and c_2 = 2485 m/s (solid lines) predicting a band gap or c_1 = 1985 m/s and c_2 = 2240 m/s (dashed lines) with a very small bandwidth. $q_{\perp}$ was computed using the refractive index n = 1.58 being the composition average of n_1 and n_2. The optical (UV−vis) transmission of the photonic film is shown in the inset.

temperature) BnW-544 being harder (higher sound velocity). Recording the dispersion normal to the film, the material's refractive index, n, can be obtained for a purely acoustic behavior; along that direction $q_{\perp}$ depends on n; n = 1.56 and 1.61 respectively for AW-445 and BnW-544. At 20 °C, c_1 = 1985 m/s for AW and c_2 = 2485 m/s for BnW within a typical error of about 1%. Linear acoustic phonon propagation is anticipated for amorphous polymers near the glass transition temperature at hypersonic frequencies,[22] and the longitudinal sound velocity (c) determines the high-frequency elastic modulus, $M = \rho c^2$, where ρ is the mass density. The modulus of BnW is slightly larger than for the glassy polystyrene (~6 GPa at 20 °C). The experimental c_1 and c_2 values with a ratio c_2/c_1 = 1.25 imply significant elastic impedance, ρc, contrast between the constituent polymers. This is a necessary condition for opening a band gap in the microphase-separated BCPs for phonon propagation along the periodicity direction.[23] In the case of sufficiently large elastic impedance contrast, even propagation normal to the periodicity can include dispersive ($q_{||}$ − dependent sound velocity) layer guided modes, as found in 1D multilayer polymer films.[24]

We examine first the phonon propagation normal to the periodicity. Figure 3a displays a single BLS spectrum for BCP-480 at $dq_{||}$ = 1.5 (periodicity d = 90 nm). The high MW BCP-1250 with longer periodicity (d = 280 nm) also conforms to this single doublet BLS spectrum at $dq_{||}$ = 4.7. The broader line shape compared to the two homopolymers can be attributed to the phonon dissipation in the rubbery AW sublayers (see Figure 6) and phonon scattering by the interphases or grains in the BCPs morphology. For low elastic impedance constrast, finite element analysis for perfectly bonded flat layers predicts an effective medium acoustic behavior only for $dq_{||} < 1$. For sufficiently large elastic contrast dispersive phonons due to the propagation in the alternating layers should be anticipated.[22,24] To reconcile the observed single acoustic effective medium behavior in the present microphase-separated high MW BCPs with $dq_{||} > 1$, a lower elastic contrast than estimated (c_2/c_1 = 1.25) from the sound velocities in the bulk homopolymers should be assumed. The extent of the modification for the elastic properties of the constituent homopolymers in the microphased BCPs can be inferred[23] from the effective medium sound velocity, $c_{||}$ = 2150 m/s in the BCPs. Using the block composition (φ_{AW} = 0.56) and the sound velocities c_1 and c_2 fixed to the corresponding homopolymer values, the theoretically estimated[23] effective medium sound velocity (= 2250 m/s) exceeds $c_{||}$ by about 5% that is larger than the experimental error (<1%). Apparently, c_1 and c_2 do not represent the two blocks in the BCPs. Yet, at least one of these values should be lower.

Turning to the propagation along the periodicity direction, the BLS spectrum of BCP-480 is a single (Stokes and anti-Stokes) doublet as shown in Figure 3. For this sample with its lattice constant (d = 90 nm) confirmed by the optical transmission (inset to Figure 4), the Brillouin zone (BZ) is at $q_{BZ} = \pi/d$ = 0.035 nm^{-1}. The theoretical band diagram of BCP-480, computed[23] for d_1 = 50 nm, d_2 = 40 nm, $\rho_1 = \rho_2$ = 1000 kg/m^3, and the values of c_1, c_2 in the two homopolymers, displays a sizable hypersonic phononic band gap along $q_{\perp}$ as indicated by the solid lines in the shaded region of Figure 4. In fact, this phononic behavior was anticipated from the photonic structure of the present BCPs, and it was one motivation for the present study. Parenthetically, the UV/vis spectrum of the BCP-480 (inset to Figure 3) shows a minimum transmission at

DOI: 10.1021/acs.macromol.5b00779
Macromolecules XXXX, XXX, XXX−XXX

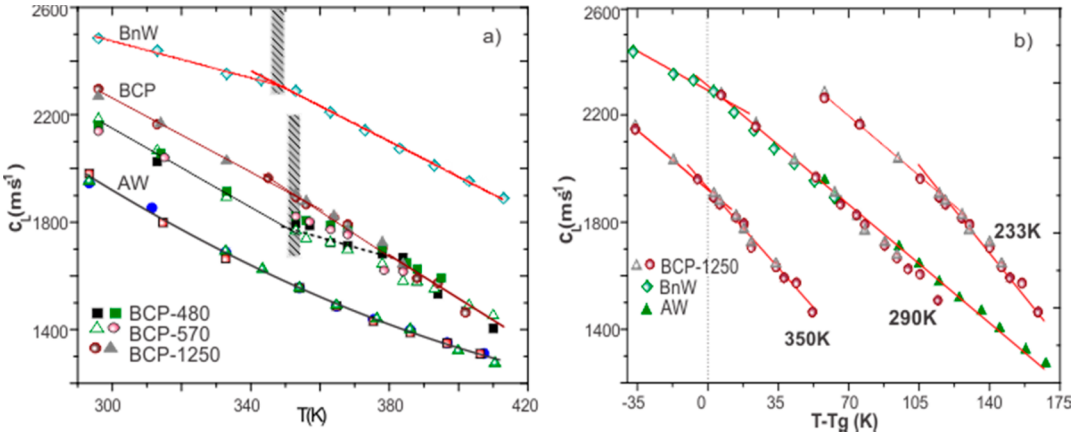

Figure 5. (a) Temperature dependence of the longitudinal sound velocity, c_L, in the two homopolymers (BnW-544 and AW-445) and three dendronized block copolymers. For the latter and AW, the data for different heating runs are shown. The shadowed line indicates the region of the glass transition. (b) The longitudinal sound velocity for the two homopolymers and one block copolymer (BCP-1250) is shown as a function of the temperature distance from T_g. For the block copolymer the low $T_{g,1}$ (= 233 K), the high $T_{g,2}$ (= 350 K), and an intermediate effective temperature (T_{eff} = 290 K) was used, as indicated in the plot.

λ = 2nd ~ 300 nm. The absence of a discernible phononic bad gap can be attributed to the modification of the elastic properties of the two BCPs relative to the corresponding bulk homopolymers, already alluded to in the case of the in-plane phonon propagation. Thus, the structure- induced material property alteration can be extracted from the phonon dispersion relation in BCP-480. In the case of the next higher MW BCP-570 with d = 162 nm, the BZ is experimentally inaccessible (Figure S1) falling into low $q_\perp$'s.

Albeit an estimation of the sound velocities in the two BCP blocks is somewhat ambiguous, the phononic bandgap closes up if, for example, c_2 is reduced by 10% while c_1 is fixed to the value of the bulk AW (above $T_{g,1}$). In this case, the computed band diagram (dashed lines in shaded region of Figure 4) shows no discernible bandgap, in agreement with the experiment. Furthermore, the computed effective medium sound velocity for in-plane phonon propagation compares well with the experimental $c_\parallel$ (= 2150 m/s). Additional information on the physical state of the two blocks can be obtained by the temperature dependence of the sound velocities in both homopolymers and BCPs and their local dynamics by BLS and DS, respectively. The sound velocity is a sensitive probe of the local chain packing, whereas segmental dynamics (subsection IIIC) reflect both local packing and the energetics of local conformational changes.

B. Thermomechanical Behavior. For the temperature-dependent BLS experiment, we selected phonon propagation normal to the periodicity at a fixed scattering angle θ = 90° and hence constant $q_\parallel$ = 0.0167 nm^{-1} to measure the in-plane effective medium longitudial sound velocity, c_L. Temperature was increased by multiple steps from room temperature to about 420 K with equlibration duration of 20 min at each temperature, and accumulation time was about 30 min per spectrum. The sound velocity, $c_L = 2\pi f/q_\parallel$, was obtained by a single Lorentzian representation of the BLS spectra (Figure S2). The temperature dependence $c_L(T)$ in the two homopolymer films is shown in Figure 5a. The high-frequency sound velocity depends on the local segmental packing which changes at the dilatometric glass temperature[17,18] as clearly observed for BnW. The glass−rubber "transition" temperature, T_{BW} =347 ± 5 K (vertical shaded stripe) was estimated from the intersection of the linear dependences (red lines in Figure 5) in the glassy and rubbery state. This value is low compared to the calorimetric value (360 K, Table 1) as DSC (Figure 2) probes the relaxation of the specific heat and usually yields a somewhat higher T_g value.[17,25] In the glass and rubbery regime the slope, $\gamma = c_L^{-1}(\partial c_L/\partial T)$ assumes values of 1.0 × 10^{-3} and 1.5 × 10^{-3} K^{-1}, respectively.

On the contrary, the sound velocity in AW drops with temperature much stronger than in BnW. Far above T_g, the drop conforms to a nonlinear dependence described by a quadratic equation $c_L = 5306(1 - 2.88 \times 10^{-3}T + 2.64 \times 10^{-6}T^2)$ (solid line in Figure 5), where T is in K and c_L in m/s. The homopolymer AW is therefore in the rubbery state, and the transition to the glass should occur below ambient temperature ($T_{g,1}$ = 233 K, Table 2). This notion is corroborated by the lower sound velocity of AW compared to the glassy BnW at ambient temperature due to the higher free volume of the former; c_L decreases with the free volume. In fact, a satisfactory superposition is observed in the plot c_L vs $T - T_g$ (Figure 5b), suggesting domination of the free volume effect, as the sound velocity assumes very similar values in the two homopolymers at temperatures equidistant from their T_g.

Figure 5a includes the $c_L(T)$ in three different BCPs at temperatures above their low $T_{g,1}$ (~233 K, Table 2) of the BCPs. In this high-temperature regime, the microphase-separated AW-block is already in the rubbery state with relatively strong temperature-dependent sound velocity (γ = 1.5 × 10^{-3} K^{-1}) resembling the slope for the AW-bulk homopolymer. In spite of this high slope already, a transition temperature, T_{BCP} = 354 ± 5 K, is discernible in the shape of $c_L(T)$ in the three BCP's films. In BCP-1250, the slope in the rubbery state increases further (γ = 1.75 × 10^{-3} K^{-1}) due to the softening of the BnW block. Note that the form of $c_L(T)$ above T_{BCP} is different (concave) than in AW (convex). In the other two BCPs, a turnover of the $c_L(T)$ occurs at about T_{BCP}. Further, the latter is somewhat lower, as in the case of BnW than T_{g2} from DSC (Figure 1 and Table 2); the sound velocities at 295 K and their temperature dependence are listed in Table S1.

An effective medium acoustic phonon is observed in the microphase-separated BCPs as the probing phonon wavelength exceeds the lamellar thickness. Nevertheless, the softening of the hard block affects the slope of the effective medium sound

DOI: 10.1021/acs.macromol.5b00779
Macromolecules XXXX, XXX, XXX−XXX

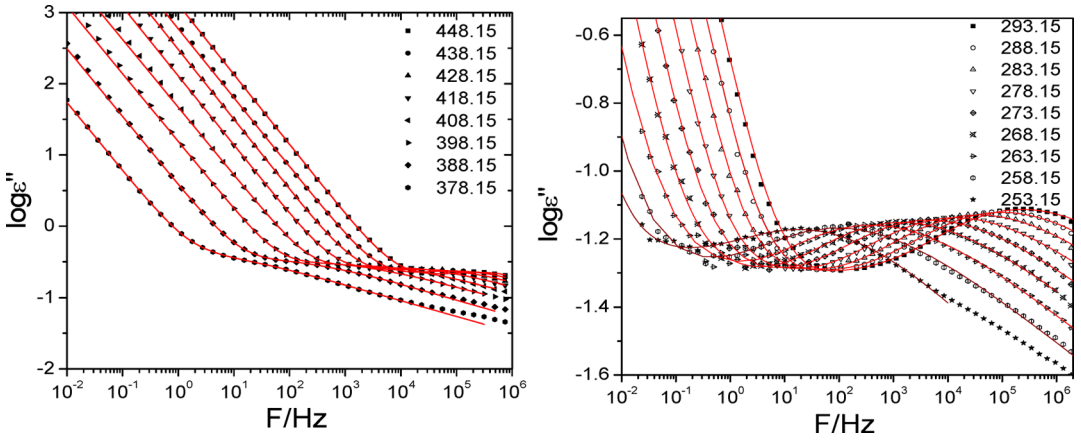

Figure 6. Dielectric loss curves of the homopolymers, BnW-789 (left) and AW-445 (right) at some selected temperatures as indicated. The lines represent the result of the fit using the HN function and the conductivity contribution (eq 1).

velocity around the second glass transition temperature $T_{g,2}$, allowing for a rough estimation of this temperature. The successful overlap for the homopolymers sound velocities, c_1 and c_2, in Figure 5b fails for a corresponding representation of the effective medium sound velocity c_L, either vs $(T - T_{g,2})$ or vs $(T - T_{g,1})$. Because of the effective medium nature of c_L, a superposition in Figure 5b is feasible only using a T_{eff} falling between the two block T_gs. In fact, the used $T_{eff} \sim 290$ K is a composition average of $T_{g,1}$ and $T_{g,2}$ justified by free-volume concepts with similar expansion coefficients for the constituent homopolymers. We should also note that below about T_{eff} the segmental dynamics associated with BnW become frozen (Figure 8).

Furthermore, Figure 5 reveals different trends for the three symmetric BCPs with very similar $T_{g,1}$ and $T_{g,2}$. BCP-1250 exhibits about 7% higher c_L (error <1%) than the two lower MW BCPs (480 and 570). The sound velocity in the latter crosses over to the high c_L state of BCP-1250 at a second crossover temperature, $T_c = 380$ K. The sound velocities above this temperature is expectedly the same for all symmetric BCPs in the equilibrium rubbery state. The observed different c_L values at $T < T_{g,2}$ should be associated with the glassy BnW block of the BCPs and to interfacial mxing. While the former might imply metastability, inherent to glasses,[27] the latter relates to confinement effects. The observation that the disparity in c_L values between the high and low MW BCPs persists even after heating the samples up to 410 K (different runs in Figure 5a) renders interfacial mixing as the most probable source. The microphase separated BCPs resemble dense polymer brushes anchored to the interface that might change the behavior of the two blocks relative to the homopolymer counterparts. The behavior of BCP-1250 suggests a sharper interface with stretched brush-like configuration. Segmental dynamics of these BCPs sensitive to packing and additionally to conformational energetic effects are addressed in the next section. In contrast to the scatterng techniques, the spatial resolution of the segmental processes, as seen in dielectric spectroscopy, is given by the intrinsic length scale associated with the liquid-to-glass transition.

C. Local Segmental Dynamics. Dielectric spectroscopy (DS) is very sensitive to the local (and global chain) dynamics provided that the molecules have—even weak—dipoles.[19,20] In the present case, both homopolymers possess sufficiently strong dipoles. However, the polymer architecture here is complex, consisting of a sterically congested array of side chains that are unified through a common backbone. The backbone and the side chains (the wedges) have dipoles that are more diluted in the AW case because of the alkyl side groups. The expectation is that in BCPs there will be several dielectrically active processes reflecting the dynamics of the phase-separated domains and possibly of the interface.

The DS results for the homopolymers are shown in Figure 6. They show the main segmental relaxation with distinctly different effective dielectric strengths, $T\Delta\varepsilon = 640$ and 200 K for BnW and AW, respectively, together with the conductivity contribution at lower frequencies. Furthermore, the low-frequency slope m, extracted from the fit to the HN function (eq 1), of the distribution of relaxation times, assumes values of 0.35 and 0.64 for AW-445 and BnW-789, respectively. These findings reveal a single—albeit broad—highly cooperative segmental process in the homopolymers despite the molecular "heterogeneity" reflected in the rigidity of the backbone and side groups. The extracted relaxation times are presented in Figure 8 together with the BCPs times.

The segmental relaxation times of homopolymers follow the non-Arrhenius (Vogel−Fulcher−Tammann) equation

$$\tau = \tau_0 \exp\left(\frac{B}{T - T_0}\right) \tag{3}$$

where τ_0 (= $\times 10^{-12}$ s held fixed in the fitting procedure) is the relaxation time in the limit of very high temperatures, B is the activation parameter, and T_0 is the "ideal" glass temperature for this process. The B and T_0 parameters assume the following values 1700 ± 30 K, 2560 ± 60 K and 184 ± 2 K, 276 ± 2 K for the AW-445 and BnW-789 homopolymers, respectively. The activation energy $E = RB$, with R being the gas constant, amounts to about 14 and 21 kJ/mol for AW and BnW, respectively. In a simplified intramolecular view of the freezing of segmental polymer dynamics at the liquid-to-glass transition (see Figure 03 in ref 28), the lower energy required for local conformational rearrangements in AW suggests higher dynamic flexibility than in BnW. The long flexible alkyl chains (in AW) effectively plasticize the backbone and lower E and the glass temperature, in comparison to the BnW block by about 130 K. This situation here is reminiscent of the internal plasticization in poly(n-alkyl methacrylates), where T_g drops by increasing the length of the side group (Figure S3). By varying this length from $n = 1$ (poly(methyl methacrylate)) to $n = 10$ (poly(decyl

DOI: 10.1021/acs.macromol.5b00779
Macromolecules XXXX, XXX, XXX−XXX

methacrylate)), the liquid-to-glass temperature is shifted by about 160 K.[30] We note that the homopolymer AW bears three decyl side group per wedge (Scheme 1) on a different backbone; hence, the observation of a similar plasticization effect (Figure S3) with the poly(*n*-alkyl methacrylates) is remarkable.

It would be now interesting to compare the temperature dependence of the segmental relaxation time in the homopolymers with other rigid and flexible polymers reported in the literature. The most widely accepted metric of the steepness of the temperature dependence of the segmental relaxation times close to the glass temperature is the fragility parameter or the steepness index, m^*, defined as[29]

$$m^* = \frac{\partial(\log \tau)}{\partial\left(\frac{T_g}{T}\right)}_{T=T_g} \quad (4)$$

which is equivalent to the slope in the "fragility" plot of log τ vs T_g/T. The steepness index can readily be calculated from

$$m^* = \frac{BT_g}{(T_g - T_0)^2(\ln 10)} \quad (5)$$

and amount to ~60 for the homopolymers. This value of the steepness index is characteristic of "fragile" glass-formers. It has been suggested that fragility is controlled by the side-group stiffness relative to the backbone.[29] For example, polymers bearing stiff backbones, such as polycarbonate and poly(ethylene terephthalate), have $m \sim 132$ and 156, respectively.[29] Similarly, polymers with relatively stiff side groups have $m \sim 100$. On the other hand, polymers with relatively flexible side groups, e.g., polyisoprene ($m \sim 60$) and polyisobutylene ($m \sim 46$), have considerably lower values that are in the observed range.[29,30] This again reflects the inhomogeneous repeat units of the homopolymers with an intermediate side-group stiffness relative to the backbone.

The DS spectrum for the BCP-3123 is shown in Figure 7 whereas the very similar dielectric spectra of the remaining copolymers are presented in Figures S4 and S5. BCPs in the strong segregation regime should display the segmental dynamics of the constituent homopolymers. Instead, the BCP dynamics are far richer than in the bulk AW and BnW, displaying four dielectrically active processes both at high and low temperatures. These are represented by two overlapping HN functions (eq 1) at higher and two at lower temperatures. The obtained relaxation times are summarized in the Arrhenius plot of Figure 8 along with the segmental relaxation times of the two homopolymers.

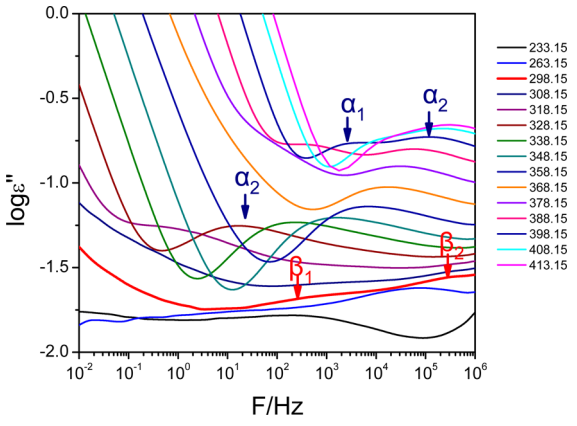

Figure 7. Dielectric loss curves of BCP-3123 at some selected temperatures as indicated. The different dynamic processes are indicated as α_1 and α_2 and β_1 and β_2.

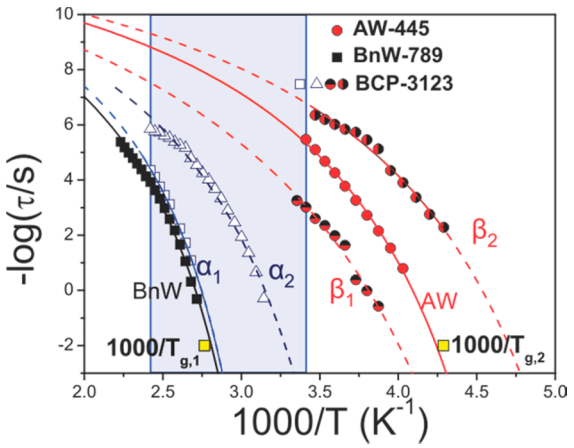

Figure 8. Arrhenius relaxation map of the multiple processes in BCP-3123 and the single α-relaxation processes in the bulk homopolymers (BnW and AW). The α_1 and α_2 processes have activation energies and relaxation times in the vicinity of BW segmental process, whereas β_1 and β_2 have characteristics corresponding to AW-445 homopolymer. The copolymer glass temperatures from DSC are also shown with the yellow squares. The blue hatched area indicates the temperature range (410−294 K) of the BLS experiment.

It is not uncommon that several cooperative processes contribute to the dielectric spectra of architecturally complex polymers comprising polar side groups.[31] Phase-separated polymer blends as well as nanophase-segregated block copolymers have two segmental processes that in the absence of an intervening glass temperature (e.g., during the process of spinodal decomposition or nucleation and growth, respectively) are identical to the homopolymer segmental dynamics.[32,33] Dynamic heterogeneity is also reported for thermodynamically miscible polymer blends and copolymers displaying two segmental processes as a result of different characteristic probing scales for the low- and high-T_g components.[34,35] These length scales can be ascribed[36] to purely intrachain contributions (i.e., to to the individual Kuhn length) due to chain connectivity effects, although intermolecular contributions cannot be excluded.[37]

The situation here is far more complex as four cooperative (i.e., VFT-like) processes appear in the dynamic window. From the four cooperative processes, the slower one (α_1), being in the vicinity of the BnW homopolymer, can be unambiguously assigned to the BnW segmental relaxation in the copolymer. According to eq 3, the strong similarity of α_1 ($B \sim 2350 \pm 30$ K, $T_0 \sim 279 \pm 2$ K) to the BnW segmental dynamics implies almost the same T_0 and activation parameter B for this component in the BCPs. The former conforms to the same T_g value in the BnW and the second $T_{g,2}$ in the BCPs (Table 2) whereas the latter implies a virtually unchanged conformational energy landscape of the BnW segments in the microphase-separated BCPs. The faster relaxation process, α_2 (Figure 7), present only in the BCPs, is considerably broader than α_1 (m = 0.3 vs 0.7) that is reminiscent of the effect of significant composition fluctuations.[38] In fact, the lower value T_0 (= 230 ±

DOI: 10.1021/acs.macromol.5b00779
Macromolecules XXXX, XXX, XXX−XXX

3 K) that describes the temperature dependence of the α_2 relaxation times (dashed line in Figure 8) implies mixing of BnW with AW segments occurring at the BCP interphase. On the other hand, the activation parameter B (= 2400 ± 60 K), being very similar for both α_1 and α_2 processes in the BCP and bulk BnW, characterizes dynamics of BnW segments in the BCP. Thus, the segmental dynamics of BnW in the BCPs are heterogeneous with slow (α_1) and fast (α_2) relaxation in virtually pure BnW and miscible BnW/AW regions.

In these miscible regions, AW segments undergo faster than α_2 but slower than in bulk AW dynamics represented by the β_1 process, as shown in Figure 8. This process, however, freezes at much lower T_0 (= 173 ± 3 K) than the fast process α_2 (T_0 = 279 K) for BnW segments in the same regions. This apparently conflicting observation can be rationalized considering the cooperative nature and the heterogeneity of segmental dynamics in two component systems near glass transition.[38,39] Assuming different cooperative volume for the low and high T_g components, BnW segmental dynamics with larger cooperativity sense an average composition, and hence higher T_0, than the more local AW segmental dynamics. The latter is predominantly affected by intrachain correlations and hence AW-rich environment with lower T_0. The additional relaxation process β_2, being faster than β_1, should be associated with AW segmental dynamics in virtually pure AW regions. It is however faster than the bulk AW segmental relaxation (Figure 8 and Figure S5) and characterized by somewhat broader distribution (m = 0.3) and lower T_0 (= 165 ± 3 K) than in the bulk AW (m = 0.35, T_0 = 184 K); similar processes have been also observed for a microphase-separated polystyrene−poly(methylphenylsiloxane) diblock copolymer.[40] The speed-up of β_2 in the BCP relative to the bulk AW can be assigned to the confined AW segmental relaxation in the diblock.[37,40] This assignment is corroborated by the relative dielectric strength of the processes in the copolymer being a fraction of the corresponding homopolymer intensities. Interestingly, although the DSC glass temperature $T_{g,1}$ couples to α_1, the broad lower $T_{g,2}$ (Table 2) couples to both β_1 and β_2 processes.

In view of the DS results of Figure 8 and Figures S4 and S5, the effective medium sound velocity, c_L, in the BCPs (Figure 5a) at temperatures above $T_{g,2}$ refers to an equilibrium melt only for the AW block. This sound velocity is therefore amenable to the segmental packing that controls the free volume but the value of c_L is spatially averaged over about the length scale of the phonon wavelength (Figure 1). The free volume rearrangements in the temperature range between 290 K and $T_{g,1}$ (~360 K) (shaded area in Figure 8) are kinetically controlled by the α_1 and α_2 processes. For the high-MW BCP, the slightly higher c_L values (by ~100 m/s) in Figure 5a at $T < T_{g,1}$ suggest more effective segmental packing or different alignment parallel to the substrate. In this context, we should note that fidelity of the lamellar morphology of the high MW polymer films is lower attributed to the higher energy barrier to assembly. The more ordered low-MW BCPs recover the high-temperature c_L value above about 350 K (Figure 5a), when the α_1 process has been activated. In the same context, the spatially average c_L in the BCPs and the homopolymers assume similar values in the plot of Figure 5b, if an effective T_g, in the vicinity of the freezing temperature of the α_2 process in the BCPs is used. Finally, in view of the strong dynamic heterogeneities (four processes in Figure 8), the conjecture of modified sound velocities for the block components in BCP compared to their bulk (c_1 and c_2 in subsection IIIA) appears realistic.

IV. CONCLUSION

The thermomechanical properties and segmental dynamics of symmetric diblock copolymers with different molar mass constructed from discrete wedge-type repeat units and the corresponding dendronized constituent homopolymers (Scheme 1) are studied by DSC, Brillouin light scattering, and dielectric spectroscopy. Up to the highest examined temperature of about 410 K, all BCPs are in the microphase-separated state exhibiting two glass temperatures ($T_{g,1}$ = 233 K, $T_{g,2}$ = 360 K) revealed by DSC and confirmed by DS and BLS techniques that probe heterogeneous segmental dynamics and the effective medium longitudinal sound velocity (c_L), respectively. The proximity of these glass temperatures to the values of the individual bulk homopolymers indicates strong segregation of the annealed BCP. Because of the vastly different T_gs, the constituent components possess different longitudinal velocities sufficient to open phononic bandgaps in these photonic BCP.

The unanticipated absence of hypersonic phononic bandgap implies reduced difference between the sound velocities (lower elastic contrast) of the two blocks compared to the corresponding values (c_1, c_2) of the constituent bulk homopolymers. This assertion is also supported by the lower c_L relatively to the effective medium sound velocity computed from the BCP composition and c_1, c_2. The latter are predominantly free volume controlled as suggested by their similar values at temperatures equidistant from T_g. In the same context, c_L of the BCP follows a superposition on the same $T - T_g$ plot, if an effective T_g intermediate between $T_{g,1}$ and $T_{g,2}$ is used. Because of the low BLS magnification and the proximity of the block sound velocities for the in-plane phonon propagation, only the effective medium c_L is resolved.

On the other hand, DS reveals heterogeneous segmental dynamics. In the homopolymers the location of the segmental dynamics and the associated glass temperature is largely controlled by the presence of flexible alkyl chains (in AW) attached on the wedges. However, the temperature dependence of the segmental dynamics exhibit "fragile" behavior, reflecting mainly the dynamics of the wedges. BCP dynamics reveal multiple cooperative processes associated with the freezing of the "segmental" dynamics of the individual blocks and additional processes associated with the interphases.

To our knowledge this is the first system comprising phase-separated, dynamically heterogeneous and confinement aspects. Future studies will explore the role of a modulated polarizability parallel and perpendicular to the electric field in relation to the four dynamic processes.

■ ASSOCIATED CONTENT

Supporting Information

Figures S1−S5. The Supporting Information is available free of charge on the ACS Publications website at DOI: 10.1021/acs.macromol.5b00779.

■ AUTHOR INFORMATION

Corresponding Author

*E-mail fytas@iesl.forth.gr (G.F.).

Present Address

G.M.M.: Department of Chemistry and Biochemistry, University of Colorado Boulder, Boulder, CO 80309.

Notes

The authors declare no competing financial interest.

DOI: 10.1021/acs.macromol.5b00779
Macromolecules XXXX, XXX, XXX−XXX

■ ACKNOWLEDGMENTS

This work was cofinanced by the E.U.-European Social Fund and the Greek Ministry of Development-GSRT in the framework of the program THALIS. The current work was supported by the Research unit on Dynamics and Thermodynamics of the UoI cofinanced by the European Union and the Greek state under NSRF 2007-2013 (Region of Epirus, call 18). The work carried out at Caltech was supported by the Camille and Henry Dreyfus Postdoctoral Program in Environmental Chemistry. A.A. thanks Elena Alonso for the technical assistance in the BLS experiment.

■ REFERENCES

(1) Bates, F. S.; Hillmyer, M. A.; Lodge, T. P.; Bates, C. M.; Delaney, K. T.; Fredrickson, G. H. *Science* **2012**, *336*, 434−440.
(2) Miyake, G. M.; Weitekamp, R. A.; Grubbs, R. H. In *Handbook of Metathesis*, 2nd ed.; Grubbs, R. H., Khosravi, E., Eds.; Wiley-VCH: Weinheim, Germany, 2015; Vol. 3, pp 93−113.
(3) Moon, J. H.; Yang, S. *Chem. Rev.* **2010**, *110*, 547−574.
(4) Edrington, A. C.; Urbas, A. M.; DeRege, P.; Chen, C. X.; Swager, T. M.; Hadjichristidis, N.; Xenidou, M.; Fetters, L. J.; Joannopoulos, J. D.; Fink, Y.; Thomas, E. L. *Adv. Mater.* **2001**, *13*, 421−425.
(5) Hustad, P. D.; Marchand, G. R.; Garcia-Meitin, E. I.; Roberts, P. L.; Weinhold, J. D. *Macromolecules* **2009**, *42*, 3788−3794.
(6) Kang, C.; Kim, E.; Baek, H.; Hwang, K.; Kwak, D.; Kang, Y.; Thomas, E. L. *J. Am. Chem. Soc.* **2009**, *131*, 7538−7539.
(7) Piunova, V. A.; Miyake, G. M.; Daeffler, C. S.; Weitekamp, R. A.; Grubbs, R. H. *J. Am. Chem. Soc.* **2013**, *135*, 15609−15616.
(8) Rzayev, J. *ACS Macro Lett.* **2012**, *1*, 1146−1149.
(9) Hu, M.; Xia, Y.; McKenna, G. B.; Kornfield, J. A.; Grubbs, R. H. *Macromolecules* **2011**, *44*, 6935−6943.
(10) (a) Verduzco, R.; Li, X.; Pesek, S. L.; Stein, G. E. *Chem. Soc. Rev.* **2015**, DOI: 10.1039/c4cs00329b. (b) Sumerlin, B. S.; Matyjaszewski, K. In *Macromolecular Engineering: Precise Synthesis, Materials Properties, Applications*; Matyjaszewski, K., Gnanou, Y., Leibler, L., Eds.; Wiley-VCH: Weinheim, Germany, 2007.
(11) Zhang, A.; Shu, L.; Bo, Z.; Schlüter, A. D. *Macromol. Chem. Phys.* **2003**, *204*, 328−339.
(12) Boydston, A. J.; Holcombe, T. W.; Unruh, D. A.; Fréchet, J. M. J.; Grubbs, R. H. *J. Am. Chem. Soc.* **2009**, *131*, 5388−5389.
(13) Miyake, G. M.; Piunova, V. A.; Weitekamp, R. A.; Grubbs, R. H. *Angew. Chem., Int. Ed.* **2012**, *51*, 11246−11248.
(14) Zhang, A.; Shu, L.; Bo, Z.; Schlüter, A. D. *Macromol. Chem. Phys.* **2003**, *204*, 328−339.
(15) Boydston, A. J.; Holcombe, T. W.; Unruh, D. A.; Fréchet, J. M. J.; Grubbs, R. H. *J. Am. Chem. Soc.* **2009**, *131*, 5388−5389.
(16) Urbas, A. M.; Thomas, E. T.; Kriegs, H.; Fytas, G.; Penciu, R. S.; Economou, E. N. *Phys. Rev. Lett.* **2003**, *90*, 108302.
(17) Cheng, W.; Sainidou, R.; Burgardt, P.; Stefanou, N.; Kiyanova, A.; Efremov, M.; Fytas, G.; Nealey, P. F. *Macromolecules* **2007**, *40*, 7283−7290.
(18) Caponi, S.; Corezzi, S.; Mattarelli, M.; Fioretto, D. *J. Chem. Phys.* **2014**, *141*, 214901−7.
(19) Kremer, F.; Schönhals, A. In *Broadband Dielectric Spectroscopy*; Springer: Berlin, 2002.
(20) Floudas, G. Dielectric Spectroscopy. In *Polymer Science: A Comprehensive Reference*; Matyjaszewski, K., Möller, M., Eds.; Elsevier BV: Amsterdam, 2012; vol. *2.32*, pp 825−845.
(21) Floudas, G.; Paluch, M.; Grzybowski, A.; Ngai, K. L. *Molecular Dynamics of Glass-Forming Systems. Effects of Pressure*; Springer: Berlin, 2011.
(22) Gomopoulos, N.; Saini, G.; Efremov, M.; Nealey, P. F.; Nelson, K.; Fytas, G. *Macromolecules* **2010**, *43*, 1551−1555.
(23) Schneider, D.; Liaqat, F.; El Boudouti, E.; El Hassouani, Y.; Djafari-Rouhani, B.; Tremel, W.; Butt, H.-J.; Fytas, G. *Nano Lett.* **2012**, *12*, 3101−3108.
(24) Cheng, W.; Gomopoulos, N.; Fytas, G.; Gorishnyy, T.; Walish, J.; Thomas, E. L.; Hiltner, A.; Baer, E. *Nano Lett.* **2008**, *8*, 1423−1428.
(25) Zhao, D.; Schneider, D.; Fytas, G.; Kumar, S. K. *ACS Nano* **2014**, *8*, 8163−8173.
(26) Charbonneau, P.; Kurchan, J.; Parisi, G.; Urbani, P.; Zamponi, F. *Nat. Commun.* **2014**, DOI: 10.1038/ncomms4725.
(27) Angell, C. A. *J. Non-Cryst. Solids* **1991**, *131*−*133*, 13.
(28) de Gennes, P.-G. *Scaling Concepts in Polymer Physics*; Cornell University Press: Ithaca, NY, 1979.
(29) Kunal, K.; Robertson, C. G.; Pawlus, S.; Hahn, S. F.; Sokolov, A. P. *Macromolecules* **2008**, *41*, 7232−7238.
(30) Floudas, G.; Stepanek, P. *Macromolecules* **1998**, *31*, 6951−6957.
(31) Grigoriadis, C.; Nese, A.; Matyjaszewski, K.; Pakula, T.; Butt, H.-J.; Floudas, G. *Macromol. Chem. Phys.* **2012**, *213*, 1311−1320.
(32) Vogt, S.; Gerharz, B.; Fischer, E. W.; Fytas, G. *Marcromolecules* **1992**, *25*, 5896−5991.
(33) Gitsas, A.; Floudas, G.; White, R. P.; Lipson, J. E. G. *Macromolecules* **2009**, *42*, 5709−5715.
(34) Kamath, S.; Colby, R. H.; Kumar, S. K.; Karatasos, K.; Floudas, G.; Fytas, G.; Roovers, J. *J. Chem. Phys.* **1999**, *111*, 6121−6128.
(35) Floudas, G.; Fytas, G.; Reisinger, T.; Wegner, G. *J. Chem. Phys.* **1999**, *111*, 9129−9132.
(36) Lodge, T. P.; McLeish, T. C. B. *Macromolecules* **2000**, *33*, 5278−5284.
(37) Harmandaris, V. A.; Kremer, K.; Floudas, G. *Phys. Rev. Lett.* **2013**, *110*, 165701.
(38) Kamath, S.; Colby, R. H.; Kumar, S. K.; Karatasos, K.; Floudas, G.; Fytas, G.; Roovers, J. *J. Chem. Phys.* **1999**, *111*, 6121.
(39) Dudowicz, J.; Douglas, J. F.; Freed, K. F. *J. Chem. Phys.* **2014**, *140*, 244905.
(40) Colmenero, J.; Arbe, A. *Soft Matter* **2007**, *3*, 1474.
(41) Vogt, S.; Gerharz, B.; Fischer, E. W.; Fytas, G. *Macromolecules* **1992**, *25*, 5896−5991.

DOI: 10.1021/acs.macromol.5b00779
Macromolecules XXXX, XXX, XXX−XXX